Atmospheric Environment 43 (2009) 869–878

Contents lists available at ScienceDirect

Atmospheric Environment

journal homepage: www.elsevier.com/locate/atmosenv

# Effect of urban morphology on wind condition in idealized city models

Jian Hang [a,*], Mats Sandberg [b], Yuguo Li [a]

[a] Department of Mechanical Engineering, The University of Hong Kong, Haking Wong Building, Pokfulam Road, Hong Kong SAR, China
[b] KTH Research School, Laboratory of Ventilation and Air Quality, University of Gävle, 801 76 Gävle, Sweden

ARTICLE INFO

*Article history:*
Received 19 May 2008
Received in revised form
22 September 2008
Accepted 21 October 2008

*Keywords:*
Wind conditions
Urban morphology
City form
Numerical simulation
Wind tunnel

ABSTRACT

Wind conditions in urban environments are important for a number of reasons. They can serve to transport air pollutants out of the urban environment and to moderate urban microclimatic conditions if satisfactory, yet can compromise pedestrian comfort and safety if not. We aim to study experimentally and numerically the effects of urban morphology (e.g., overall city form (skyline), street orientation, and street configuration) on wind conditions in cities. This report considers our initial investigations of two idealized city forms that are coincidentally similar to ancient Roman cities that were organized on one or two primary streets – a main north–south street, the *cardus maximus*, and a secondary east–west street, the *decumanus maximus* – and contained within a well-defined perimeter.

We first consider round and square city models with one main street set parallel to the approaching wind and a secondary street producing an intersection at city centre. Not surprisingly, wind conditions in the two city models are dissimilar due to their shape differences. We then consider a long rectangular city model with a fully developed steady flow region along the main street. If the main street of the round city model is narrow, the parallel approaching wind cannot blow through the entire street and a penetrating inflow exists at the leeward opening. For the round city model with two crossing streets, a slightly non-parallel wind to the main street generates a stronger wind level in the entire street volume.



## 1. Introduction

Given the current rate of urbanization and the unprecedented scale of urban development in the developing countries of the world, urban environmental quality is becoming an increasingly important concern. Industrial, commercial, institutional and residential activities and the transport vehicle emissions related to these activities combine to create urban air pollutant levels in some of these cities (Fenger, 1999) that can no longer be diluted by local winds. Understanding the relation between urban morphology and favourable wind conditions in such cities provides one key means to avoid serious urban air pollution episodes and, thereby, to improve the quality of life in urban environments in general.

Previous urban wind research has investigated turbulent flow patterns around isolated buildings (Li and Stathopoulos, 1997; Cowan et al., 1997), turbulent flow conditions in different street canyon models (Oke, 1988; Xie et al., 2006), and wind conditions in finite groups of buildings or actual urban area. For the latter, the studies can be divided into two groups – one group treats buildings as roughness elements within cities and studies the interaction between urban roughness, urban airflows and atmospheric boundary layer characteristics, the second group investigates urban airflow more microscopically within street canyons and urban canopy.

Within the first group, Grimmond and Oke (1999) reviewed and analyzed wind profiles in various urban areas and summarized available roughness parameter models. Macdonald (2000) modified a simple model for vegetative canopy flow to model urban canopy flows over arrays of cubes with low packing densities. Cheng and Castro (2002) found that staggered cube arrays generated greater drag to the wind than aligned cube arrays at the same flow condition and random height roughness produced greater surface stress than that produced by a uniform surface. Belcher et al. (2003) developed an idealized model for the adjustment of turbulent flow within canopies of sparse building arrays and for velocity reduction through such canopies and later extended this model to inhomogeneous canopies (Conceal and Belcher, 2005).

Within the second group, microscopic details of the complex turbulent flow within arrays of buildings or urban area have been studied numerically and experimentally by a number of investigators (Soulhac, 2000; Hanna et al., 2002; Chang and Meroney, 2003; Hamlyn and Britter, 2005). Cheng et al. (2003) suggested the $k$–$\varepsilon$ Reynolds-averaged Navier–Stokes (RANS) turbulence models and the Reynolds stress turbulence model (RSM) provides

* Corresponding author. Tel.: +852 2859 2625; fax: +852 2858 5415.
*E-mail address:* liyg@hku.hk (J. Hang).

1352-2310/$ – see front matter Crown Copyright © 2008 Published by Elsevier Ltd. All rights reserved.
doi:10.1016/j.atmosenv.2008.10.040

**Nomenclature**

| | |
|---|---|
| $A_O$, $A_{roof}$ | area of street opening and street roof |
| $C_p$ | pressure coefficient |
| $k$, $\varepsilon$ | turbulence kinetic energy and its dissipation rate |
| $I$ | turbulence intensity |
| $\sigma_w$ | fluctuation velocity |
| $H$, $L$, $W$ | street height, street length and street height |
| $\vec{n}$ | normal direction of street opening or roof |
| $Q_\infty$ | reference flow rate far upstream |
| $Q^*$ | normalized flow rate through street opening or street roof |
| $Q^*_{turb\pm}$ | normalized effective flow rate through open roof by turbulent exchange |
| $\overline{u}, \overline{w}$ | horizontal velocity in the $x$ direction and vertical velocity in the $z$ direction |
| $\overline{u}_\infty$ | horizontal velocity at far upstream |
| $u''$, $v''$, $w''$, | horizontal, spanwise, vertical velocity fluctuations |
| $\nu$ | kinematic viscosity of air |
| $\vec{V}, V(x,y,z)$ | velocity vector and velocity magnitude (wind speed) |
| $V^*_\infty$ | reference velocity far upstream |
| $<V^*>$ | normalized spatial mean velocity in a given volume |
| $<Q^*>$ | normalized spatial mean $Q^*$ in a given volume |
| vol | a given volume |

acceptable modeling approaches when compared to Large-eddy-simulation (LES) methods considering both solution accuracy and computational demands.

Here we propose a third approach – to model cities as obstacles characterized by an overall city form, building area density and street configuration (see Fig. 1), morphological characteristics that affect the structure and the intensity of wind entering, leaving, and flowing around and above cities. Studies of the impact of urban morphology on urban airflow are rare, although, ironically, this approach to understanding urban design was promoted by Vitruvius in the first century BC (Vitruvius, 1960). Skote et al. (2005) qualitatively investigated the flow pattern in round compact cities with one or two larger main streets. To initiate this study of urban form and airflow, two simple city forms are considered in this paper – a round city form and a rectangular city form each with a single or two intersecting main streets that dominate the otherwise compact city form. While hypothetical, given the current state of urban design globally (see Fig. 1), these simple forms have Roman precedents, as shown in Appendix A (Fig. A.1), and may be used to characterize at least the core of some smaller contemporary cities such as Gävle, Sweden (which has a primary north–south street, Kungsgatan or Kings Street, and a primary east–west street, Drottninggatan or Queen Street).

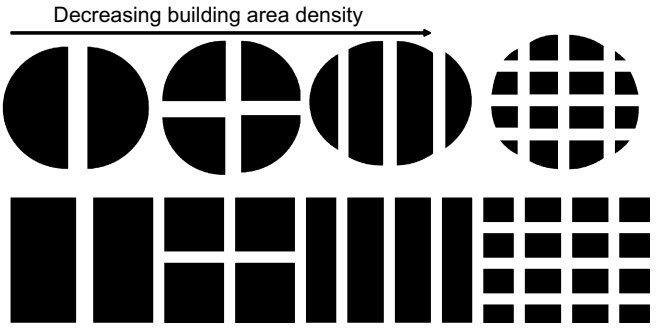


**Fig. 1.** Variation of urban form and building area density of compact cities.

## 2. Methodology

Our experiments were conducted in a closed-circuit boundary layer wind tunnel at the University of Gävle with a working section 11 m long, 3 m wide and 1.5 m high. The height of all the idealized city models used in wind tunnel was $H = 0.069$ m (Fig. 2). The round and square city models were equally divided into two or four sections by a main street (street height/street width or aspect ratio, $H/W = 1$; street length/street height ratio, $L/H = 6$) or two perpendicularly crossing streets (a main and secondary streets, $H/W = 1$, $L/H = 7$). A round city model with one narrow street ($H/W = 6.67$; $L/H = 6$) and a rectangular long city model ($H/W = 1$; $L/H = 21.7$) were also studied with an approaching wind set parallel to the main street. For the round city model with two streets, the approaching wind was set either parallel to the main street or at an angle of 15°, 30° or 45°. A total of 9 test cases were studied. Each test case is identified here as Shape [number of streets, street length ratio, aspect ratio $H/W$, wind direction]. For example, Round [1, 6, 1, 0] refers to a test case of a round city model with one street, street length ratio ($L/H$) of 6, aspect ratio ($H/W$) of 1 and wind direction of 0°. The other 8 test cases are Round [1, 6, 6.7, 0], Round [2, 7, 1, 0], Round [2, 7, 1, 15], Round [2, 7, 1, 30], Round [2, 7, 1, 45], Square [1, 6, 1, 0], Square [2, 7, 1, 0], and Long [1, 21.7, 1, 0]; see Fig. 2.

The vertical profiles of both velocity and turbulence intensity were measured far upstream (not shown). The pressure coefficient ($C_p$) on the wind tunnel floor was recorded at 400 points on a uniformly distributed grid of 20 rows and 20 columns spaced at 37 mm covering an area around and through the city models. A relatively high velocity of 19 m s$^{-1}$ in free flow was used in the wind tunnel tests for easy detection of pressure (Reynolds number $\overline{u}_\infty H/\nu = 8975$). The reference pressure ($C_p = 1$) was taken as the measured static pressure at stagnation on a solid round city model without streets at a height of $z = 0.7H$. Velocity and turbulence intensity were measured using hotwire anemometers along the street centerline at $z = 0.11H$.

For CFD simulations, the CFD code Fluent 6.2 was used with either the standard $k$–$\varepsilon$ (Launder and Spalding, 1974) or the RNG (Choudhury, 1993) $k$–$\varepsilon$ turbulence models to estimate mean flow and turbulence characteristics for stationary, incompressible, and isothermal flow conditions. The computational domain was chosen to be $81H$ long, $30H$ wide and $15H$ high with the centre of city model located at $29H$ from the upstream inlet. When the approaching wind was set parallel to the main street the symmetric half of the flow domain was analyzed. Non-slip wall boundary conditions were used at all solid surfaces. Approach wind velocity ($\overline{u}$) and turbulence intensity ($I$) profiles measured in the wind tunnel studies were used as boundary conditions at the upstream boundary of the CFD simulations and a zero normal gradient for all boundary variables was used at outflow and symmetry boundaries. The total number of grid points used was between half and one million with finer grids close to the solid surfaces. Grid refinement tests were carried out by locally refining the grids close to surfaces and found to produce little change in the predicted results.

To quantify the variation of air motion, we normalized horizontal ($x$) or vertical ($z$) velocity components by the velocity measured at the same height far upstream. Volumetric flow rates entering streets and flowing through street networks largely determine the pollutant dilution by wind flows, so we defined a reference flow rate ($Q_\infty$), Eq. (1), then utilize it to normalize the mean flow rates through openings and roofs, Eq. (2), and the

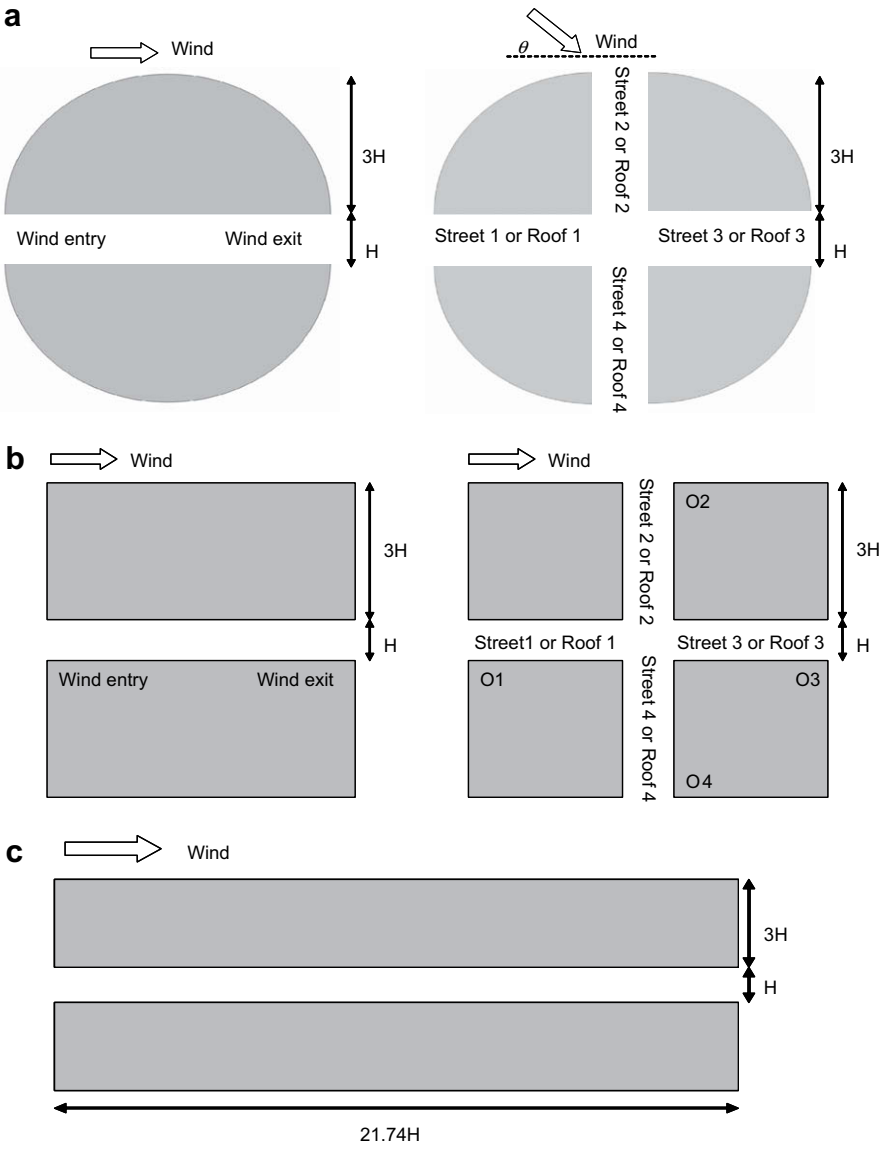


**Fig. 2.** Simple city models used in this study. (a) Round city, (b) square city and (c) long rectangular city. $H$ is the height of idealized model and $\theta$ is the angle between the approaching wind and street centerline.

effective flow rate through roofs due to turbulent exchange, Eq. (3), as defined in Li et al. (2005).

$$Q_\infty = \int_{A_O} \overline{u}_\infty \, dA = V_\infty^* \times A_O \tag{1}$$

$$Q^* = \int_A \vec{V} \cdot \vec{n} \, dA / Q_\infty \tag{2}$$

$$Q^*_{\text{turb}\pm} = \pm \int_{A_{\text{roof}}} 0.5 \, \sigma_w dA / Q_\infty \tag{3}$$

where in Eq. (1), $\overline{u}_\infty$ is the horizontal velocity far upstream, $A_O$ is the area of opening and $V_\infty^*$ is the reference velocity; in Eq. (2), $\vec{V}$ is velocity vector, $\vec{n}$ is the normal direction of a surface (street openings or roof), $A$ is the area of roof or openings; in Eq. (3), $\sigma_w = \sqrt{\overline{w''w''}} = \sqrt{2k/3}$ is the fluctuation velocity on the street roof based on the approximation of isotropic turbulence where $(u'' = v'' = w'')$ given $u''$, $v''$, $w''$ are the horizontal, spanwise, vertical velocity fluctuations and $k = (\overline{u''u''} + \overline{v''v''} + \overline{w''w''})^{1/2}$ is turbulent kinetic energy at the street roof $A_{\text{roof}}$.

To study the variation of flow rate along the main street (i.e., considering the practical difficulties of obtaining the detailed horizontal profile of street flow rates in Fluent 6.2) we divided the main street into several sections and calculated the spatial average value of the normalized horizontal flow rate in each section (see Eq. (4)). In cases with two crossing streets, we divided the whole street volume into five sections (Street 1, Street 2, Street 3, Street 4, Intersection), as shown in Fig. 2. The normalized spatial mean velocity in each section was calculated to estimate the strength of wind in different city models for purposes of comparison (see Eq. (5)).

$$< Q^* > = \frac{1}{\text{vol}} \iiint_{\text{vol}} \overline{u} dx dy dz / Q_\infty \tag{4}$$

$$< V^* >= \frac{1}{V_\infty^*}\frac{1}{\mathrm{vol}}\iiint_{\mathrm{vol}} V(x,y,z)\mathrm{d}x\mathrm{d}y\mathrm{d}z \quad (5)$$

where $V$ is the velocity magnitude, $V_\infty^*$ is defined by Eq. (1) and vol is a given volume in each section (e.g., in the entire space, $0 \geq z \geq H$, or at a low level, $0 \geq z \geq 0.13H$).

## 3. Results and discussion

CFD simulations were validated using the pressure coefficient ($C_p$) measured on the ground at the 400 grid points and the velocity (turbulence intensity) profiles measured along street centerlines for all 9 test cases. Here, we only show some example comparisons. Fig. 3a and b shows the predicted and measured 400 values of $C_p$ for the test case Round [2, 7, 1, 0]. Fig. 3c and d shows $C_p$ distribution along line K for test cases of Round [2, 7, 1, 15] and Round [2, 7, 1, 45], which corresponds, respectively, to the best and worst agreement between the numerical and measured data. Fig. 3e and f compared, measured and predicted velocity and turbulence intensity for the test case Square [2, 7, 1, 0]. Overall, there is generally a good agreement between the measured and predicted $C_p$ and velocity distribution along the principal street, however, the predicted $C_p$ distribution along the secondary streets and turbulence intensity are poorly predicted by CFD although the general trends of variation are captured.

### 3.1. Effect of overall city form for the single street city model

Fig. 4a and b shows the 3D streamlines viewed from above for two test cases Round [1, 6, 1, 0] and Square [1, 6, 1, 0]. The approaching wind can either enter the streets, or flow above or around the city model. The wake flows are obviously different for the round and square city models. The streamlined flow around the round city model generates much smaller flow separation and swirling flows than those in the case of the square city model. Fig. 4c–f shows different predicted flow quantities along the street in the three city models to explain the process of wind approaching, entering, and flowing through the street of such idealized city models. The street entry is at $x = 0$. The wind first slows down as it approaches the city model due to the obstruction

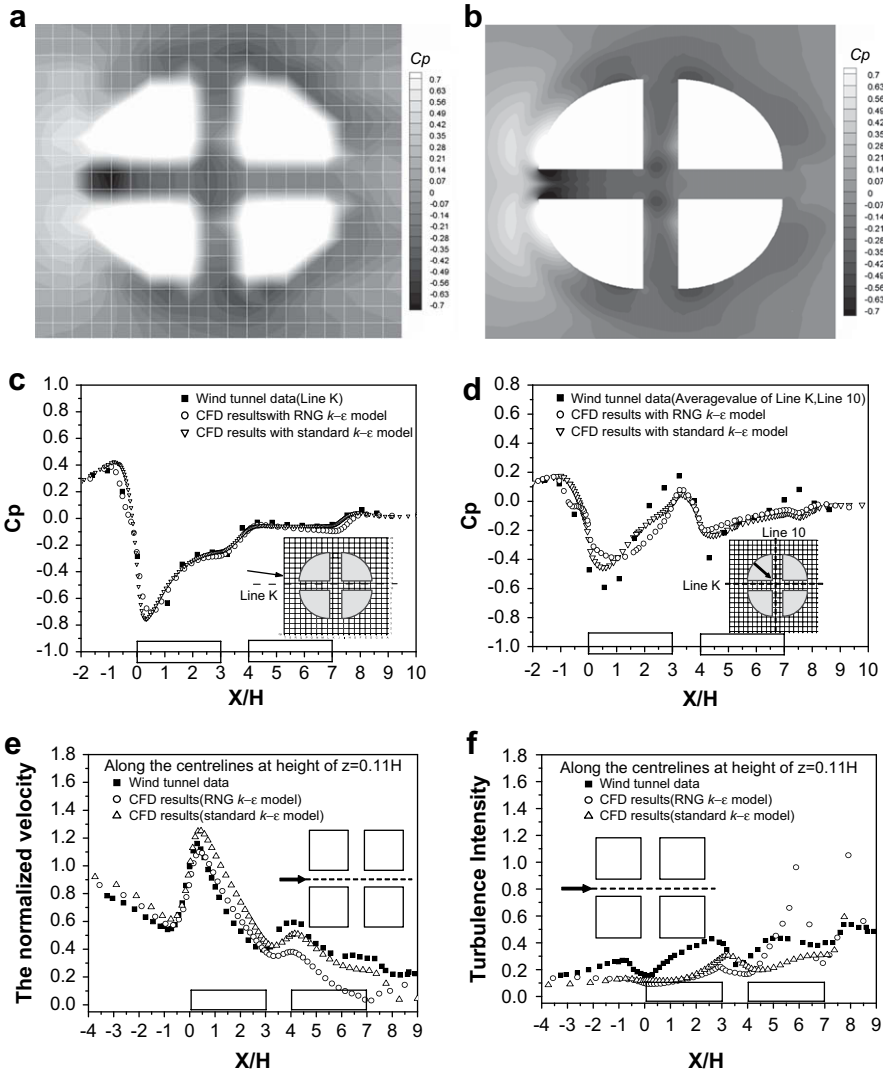


**Fig. 3.** Comparison between CFD results and wind tunnel data. (a) Measured pressure coefficient on wind tunnel floor at 400 points and (b) numerical results of $C_p$ distribution on ground for the test case Round [2, 7, 1, 0]. (c) $C_p$ distribution for the test case Round [2, 7, 1, 15]. (d) $C_p$ distribution for the test case Round [2, 7, 1, 45]. (e) Normalized centerline velocity for the test case Square [2, 7, 1, 0] and (d) turbulence intensity along the centerline for the test case Square [2, 7, 1, 0]. Each test case is identified here as Shape [number of streets, street length, aspect ratio $H/W$, wind direction].

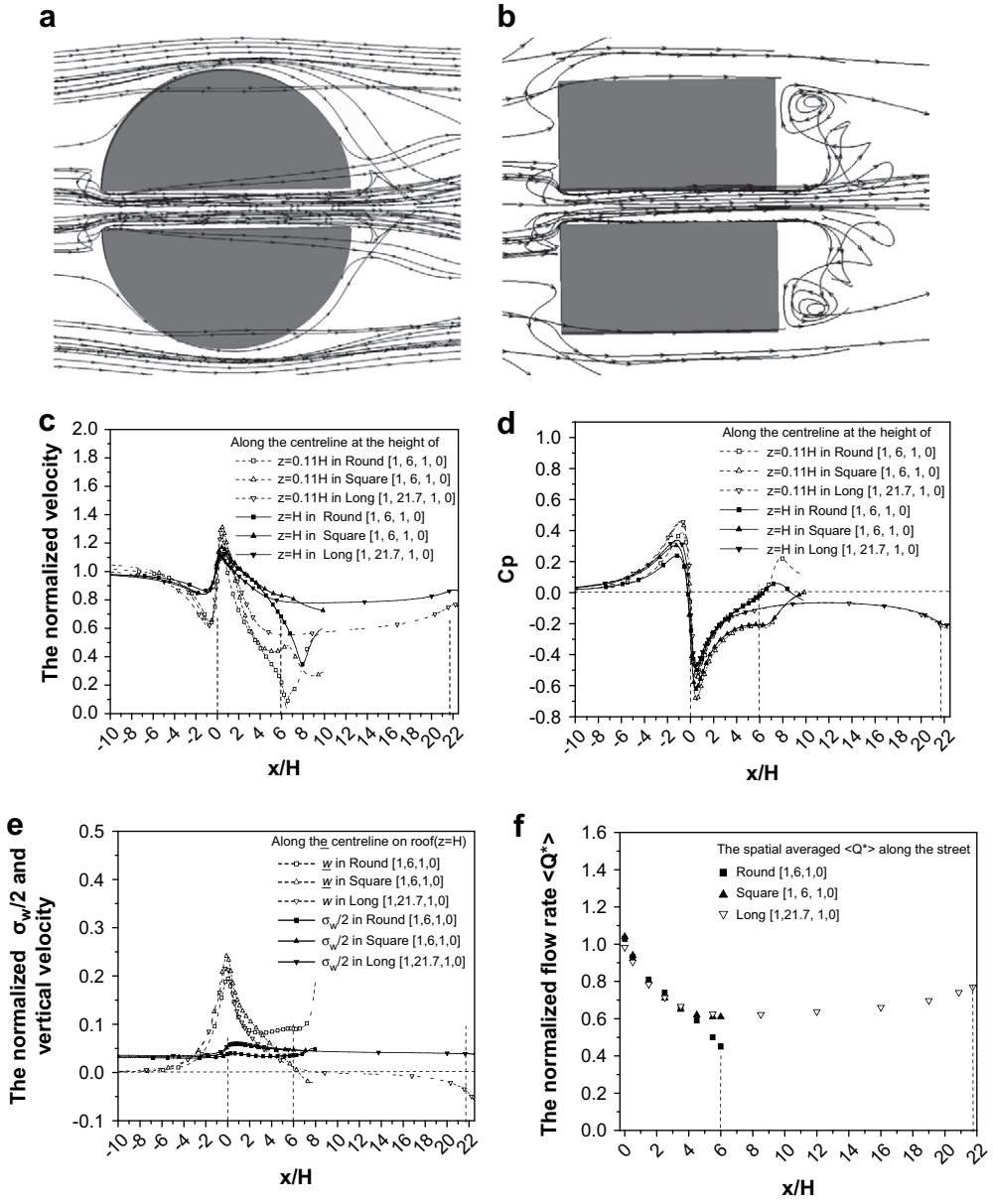


**Fig. 4.** Three-dimensional streamline in two test cases. (a) Round [1, 6, 1, 0], (b) Square [1, 6, 1, 0]. Predicted flow quantities for three test cases, i.e. Round [1, 6, 1, 0], Square [1, 6, 1, 0] and Long [1, 21.7, 1, 0], (c) the normalized velocity along the centerline, (d) pressure coefficient along the centerline, (e) the normalized $\sigma_w/2$ and $\overline{w}$ along the centerline on open roof ($z = H$), and (f) the normalized horizontal flow rate along the street ($x = 0$ is windward entry, $\sigma_w = \sqrt{2k_{roof}/3}$ is vertical fluctuation velocity on roof, $\overline{w}$ is vertical velocity). Each test case is identified here as Shape [number of streets, street length, aspect ratio $H/W$, wind direction].

of the solid wall, then it accelerates between $-0.5H$ and $0.5H$ with a strong pressure gradient and large vertical velocity (Fig. 4c–e). The normalized flow rate at street entry is close to unity for all studied situations (Fig. 4f). Some air leaves the street cavity upwardly through the street roof as it moves forward along the street. This is confirmed by the positive vertical velocity shown in Fig. 4e. Hence the wind speed and horizontal flow rate along the street decrease; see Fig. 4c and f. We also find the velocity and horizontal flow rate near leeward entry ($x/H$ from 4 to 6) of the round city model is less than that of square city model in the same region due to the stronger blockage in the wake of the round city model.

For a very long rectangular city model (Long [1, 21.7, 1, 0]), there exists a fully developed region ($x/H$ from 6 to 16), where the wind speed remains nearly constant and the pressure gradient is zero (Fig. 4c and d). Fig. 4e shows that the vertical motion is very weak at the roof level of the fully developed region in Long [1, 21.7, 1, 0] ($x/H$ from 6 to 16) and air exchange depends mainly on the turbulent exchange. The flow equilibrium between the shear stress imposed by the external wind above the roof level and the opposing friction at wall surfaces in the street cavities can be predicted in this region. Close to the leeward entry ($x/H$ from 16 to 21.7) in Long [1, 21.7, 1, 0], the negative vertical velocity at the roof level shows a downward air motion, so the horizontal flow rate increases a little; see Fig. 4e and f.

### 3.2. Effect of overall city form in the two-street city model

For the two-street city model a helical inflow in the secondary street of square city model is formed flowing from opening O2 and O4 to the city centre, as shown in Fig. 5a and c. For the round city model, on the other hand, a helical outflow forms in the secondary street flowing from the city centre to openings O2 and O4; see

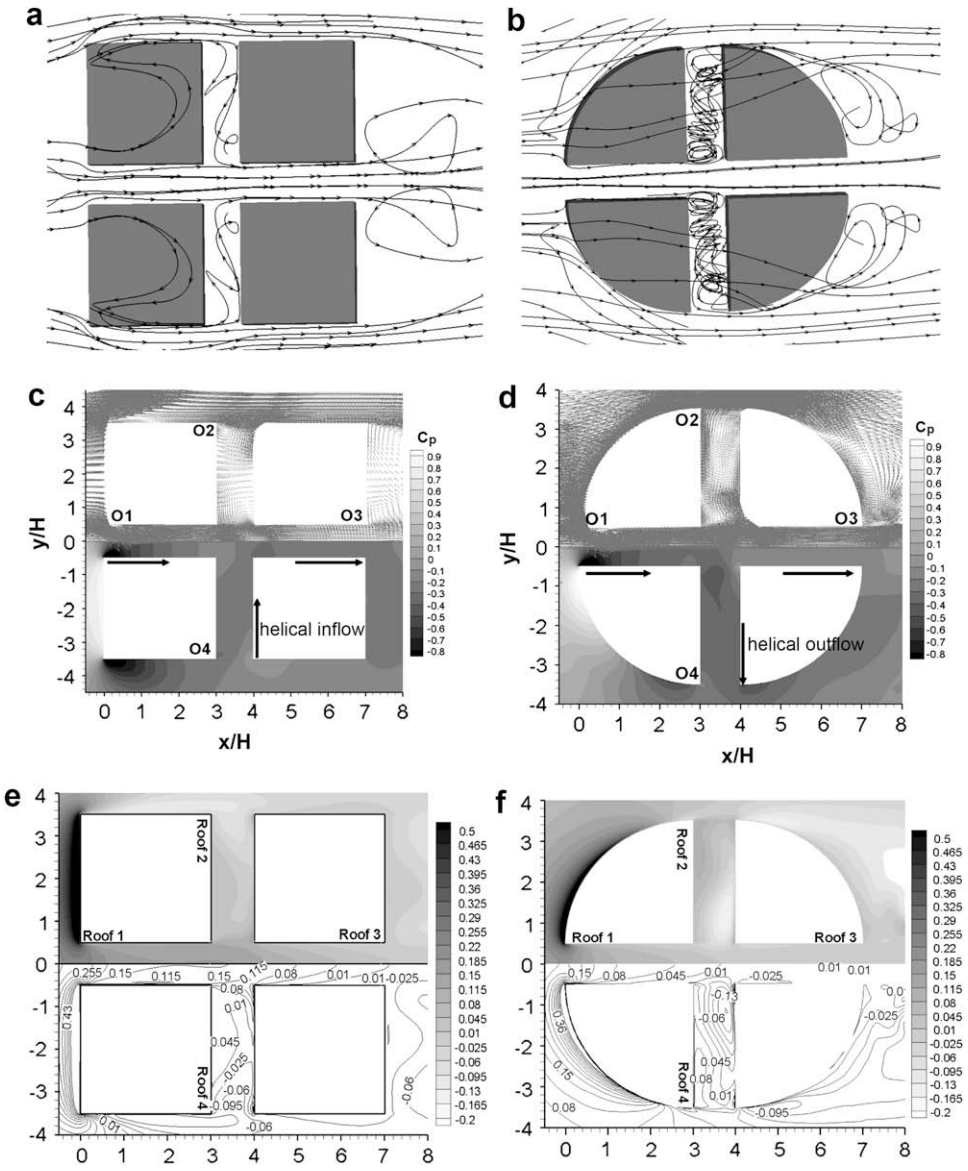


**Fig. 5.** In the cases Square [2, 7, 1, 0] and Round [2, 7, 1, 0]. (a) and (b) The three-dimensional streamline; (c) and (d) $C_p$ distribution and velocity vector in plane of $z = 0.5H$. (e) and (f) Normalized vertical velocity contour on roof level at $z = H$. $x = 0$ is windward entry. Each test case is identified here as Shape [number of streets, street length, aspect ratio $H/W$, wind direction].

Fig. 5b and d. These differences can be attributed to the distinct wake flows of the two city forms. The square city model is located within the wake generated by the city itself, while the round city model is surrounded by airstreams that generate lower pressures in the ambient than in the secondary street; see Fig. 5c and d. We divide the entire street cavity and the entire street roof into five sections as shown in Fig. 2. Street 1 (Roof 1), Street 3 (Roof 3) and Intersection belong to the main street; Street 2 (Roof 2) and Street 4 (Roof 4) are for the secondary streets. Fig. 5e and f shows the normalized vertical velocity at the roof level. There are both upward and downward motion through Roof 2 and Roof 4 due to the helical flow in Street 2 and Street 4. The upward vertical velocity on roof of the square city model is larger than that of the round city model.

Such observations can also be seen from the calculated overall flow rates through the four openings (O1, O2, O3, O4) and the entire street roof in Table 1. The notation used to define these openings is shown in Fig. 2. In Table 1, for each city model, the total positive

**Table 1**
Normalized flow rate through openings and the entire open roof.

| Test cases | The normalized flow rate $Q^*$ through openings and street roof | | | | | | | |
|---|---|---|---|---|---|---|---|---|
| | O1 | O2 | O3 | O4 | Roof (+) | Roof (−) | Roof | Roof (turb) |
| Round [2, 7, 1, 0] | 1.04[a] | −0.07 | −0.75 | −0.07 | 0.29 | −0.43 | −0.15 | ±0.58 |
| Square [2, 7, 1, 0] | 1.01 | 0.09 | −0.37 | 0.09 | 0.11 | −0.94 | −0.83 | ±0.94 |

[a] Positive values indicate inflow to the street and negative for the outflow from the street. Roof (+), Roof (−), Roof, Roof (turb) are downward inflow, upward outflow, mean vertical flow rates and the effective flow rate by turbulent exchange on the entire street roof.

**Table 2**
Normalized spatial mean velocity $<V^*>$ in the entire street height from 0 to $H$ and at a low level from 0 to $0.13H$ above the ground in each section.

| Round [2, 7, 1, 0][a] | Street 1 | Intersection | Street 3 | Street 2 | Street 4 | Entire street |
|---|---|---|---|---|---|---|
| $z$ from 0 to $H$ | 0.89 | 0.78 | 0.71 | 0.27 | 0.27 | 0.56 |
| $z$ from 0 to $0.13H$ | 0.63 | 0.44 | 0.38 | 0.36 | 0.36 | 0.43 |
| Square [2, 7, 1, 0] | Street 1 | Intersection | Street 3 | Street 2 | Street 4 | Entire street |
| $z$ from 0 to $H$ | 0.75 | 0.50 | 0.41 | 0.19 | 0.19 | 0.39 |
| $z$ from 0 to $0.13H$ | 0.43 | 0.25 | 0.19 | 0.26 | 0.26 | 0.28 |

[a] Each test case is identified here as Shape [number of streets, street length, aspect ratio $H/W$, wind direction].

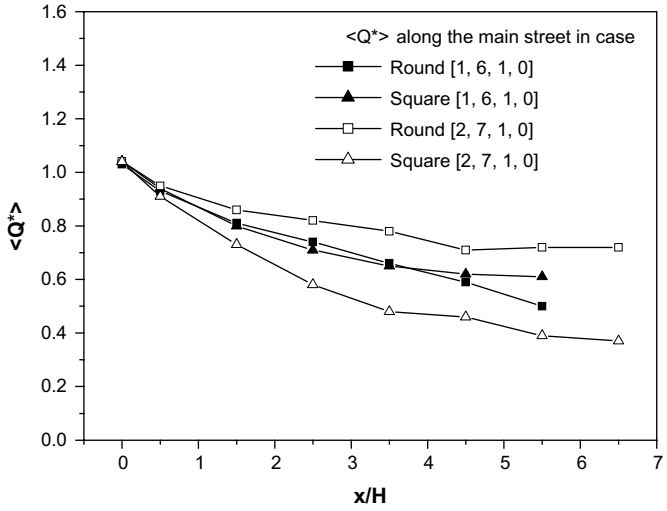


**Fig. 6.** The CFD predicted spatial average value of normalized horizontal flow rate along the main street in cases Round [1, 6, 1, 0], Round [2, 7, 1, 0], Square [1, 6, 1, 0] and Square [2, 7, 1, 0]. $x = 0$ is windward entry. Each test case is identified here as Shape [number of streets, street length, aspect ratio $H/W$, wind direction].

flow rates (i.e. inflow to the street) equal the total negative flow rates (i.e. outflow). The normalized flow rates at O1 are 1.04 and 1.01 for the round and square city models, respectively, both are slightly greater than unity, i.e. the inflow is greater than the reference flow rate far upstream. Due to symmetry, the flow rates through O2 and O4 are equal, however, airflow rates through the two side openings O2 and O4 are negative (i.e. outflow) for the round city model yet positive (i.e. inflow) for the other. Table 1 also provides the upward outflow (negative) rate, the downward inflow (positive) rate, the mean vertical flow rate and the effective flow rate by turbulent exchange on the entire street roof. In the square city model, the upward flow rate (−0.94) is much larger than the downward flow rate (0.11), however, in the other, the upward flow rate (−0.43) is only slightly greater than the downward flow rate (0.29). The total effective flow rate due to turbulent exchange in both round (±0.58) and square (±0.94) city models is larger than the mean vertical flow rate on roof, showing turbulence is important for air exchange.

Table 2 shows the spatial mean velocity in the five sections for the entire space, i.e. from $z = 0$ to $z = H$, and at a low level, i.e. from $z = 0$ to $z = 0.13H$. The spatial mean velocity in the round city model is higher than that in the square city model in each section. It is interesting to find that the spatial mean velocity at the low level near ground is greater than that over the entire space in the secondary street (Street 2 and Street 4) for both round and square city models. It shows that there is a relatively strong wind near ground of the secondary street, was an observation also reported qualitatively in Skote et al. (2005).

Finally, contrast to this is the city model with one street. Our numerical results (see Fig. 6) show that for the city model with two crossing streets the horizontal flow rate along the main street in the square city model is weakened as there is a strong street roof level outflow, while for the round city model the horizontal flow rate along the main street is strengthened a bit.

### 3.3. Effect of aspect ratio in the single street round city model

For the wind flow in an idealized city model, the external wind above the roofs acts as a motor and the friction in the city model as a kind of resistance. We divide the entire street cavity into six sections uniformly and calculate spatial mean value of horizontal flow rate along the street. Fig. 7 shows that if the main street of the round city model is too narrow ($H/W = 6.7$), i.e. test case Round [1, 6, 6.7, 0], the forward flow cannot blow through the entire street. The air that flows around two sides of the round city model collides in the wake region, entering the street through the leeward opening. This may be explained as follows. In a round city model

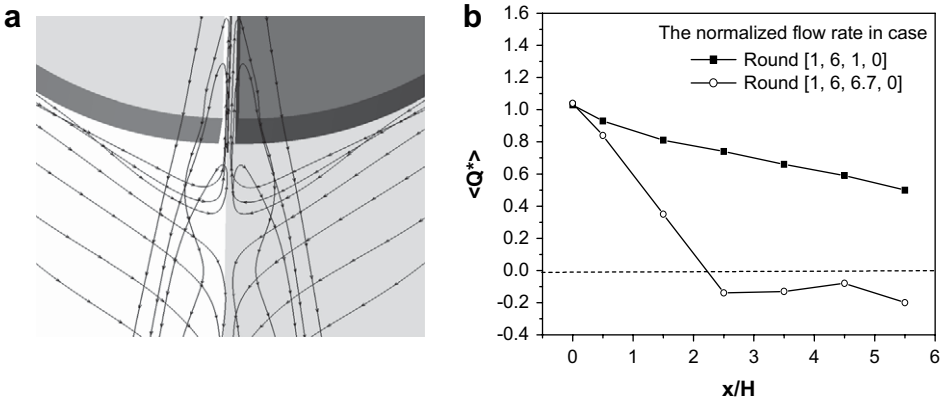


**Fig. 7.** (a) Three-dimensional streamlines at the leeward side of the narrow city for Round [1, 6, 6.7, 0] and (b) the normalized horizontal flow rate along the street $<Q^*>$ for two cases Round [1, 6, 6.7, 0] and Round [1, 6, 1, 0]. $x = 0$ is windward entry. A negative value denotes backward flow. Each test case is identified here as Shape [number of streets, street length, aspect ratio $H/W$, wind direction].

**Table 3**
Normalized flow rate $Q^*$ through street openings and the roof in Round [1, 6, 6.7, 0].

| The normalized flow rate at: | Windward opening | Leeward opening | Entire street roof |
|---|---|---|---|
| Round [1, 6, 6.7, 0][a] | 1.06 | 0.31 | −1.40 |

[a] Each test case is identified here as Shape [number of streets, street length, aspect ratio $H/W$, wind direction].

with a narrow street, the momentum flux in the airstream entering the windward entry is reduced significantly by the strong friction at the solid walls. A reduced forward momentum flux can carry the flow only so far, thus an inflow into the leeward entry from the near wake behind the city model is established.

In Table 3, the airflow rates are summarized through the two street openings and the roof. It is shown that for the narrow street (Round [1, 6, 6.7, 0]) the flow rate through both windward and leeward openings is positive (1.06 and 0.31), indicating that both flows are inward. The flow through the roof is negative (−1.40), indicating an overall upward flow through the roof. Inward flows through both ends of the streets will bring the airborne pollutants to the street centre, before extracting from the street by the upward flow through street roof. It may be argued that such a flow pattern is undesirable for pollutant removal.

### 3.4. Effect of wind direction on a two-street round city model

Four different wind angles were studied for the round city model with two crossing streets. Fig. 8 shows the three-

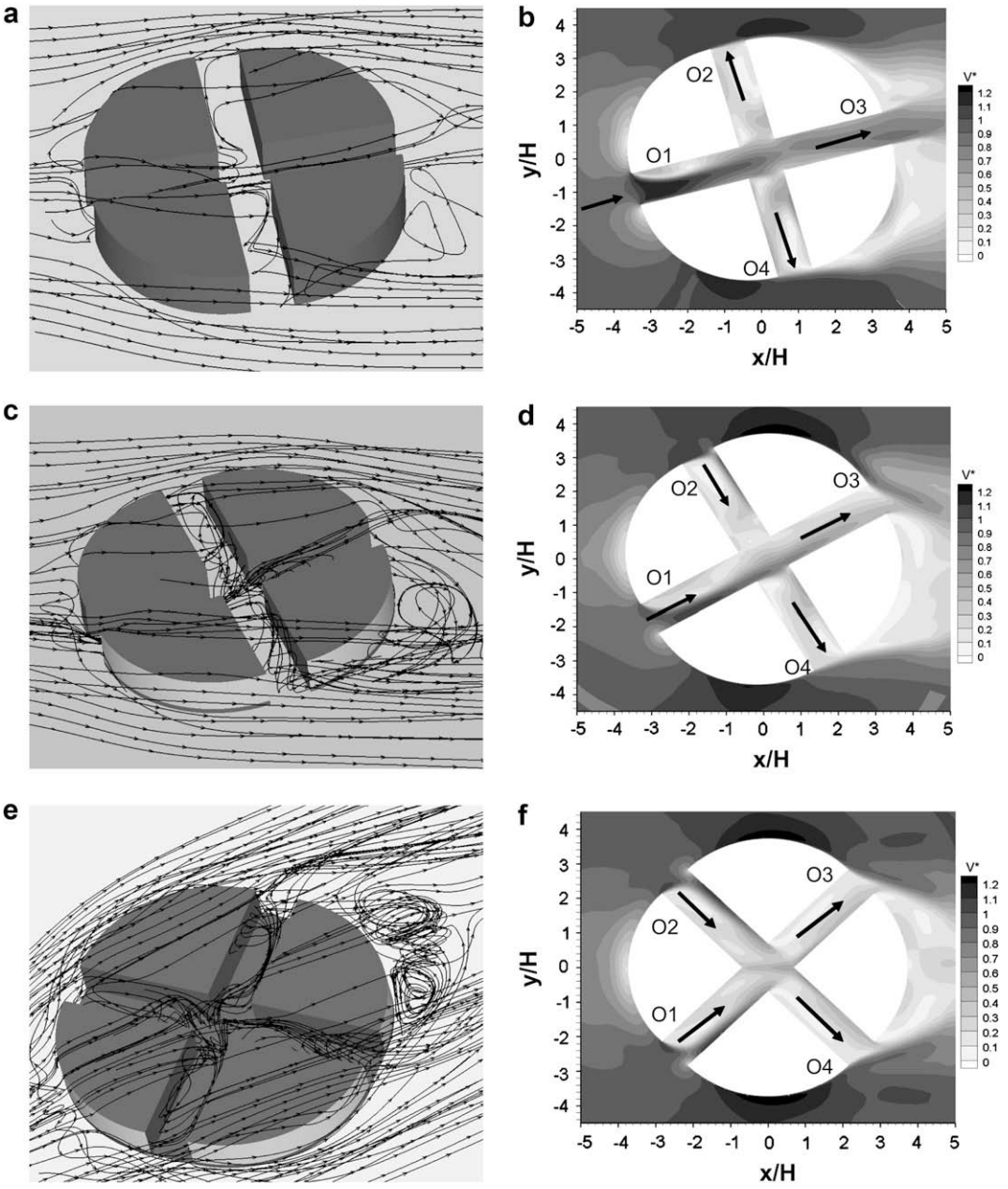


**Fig. 8.** Three-dimensional streamline (a) (c) (e) and normalized velocity distribution in plane of $z = 0.5H$ (b), (d) and (f) in the cases with wind at angles of 15°, 30° and 45° (Round [2, 7, 1, 15], Round [2, 7, 1, 30], Round [2, 7, 1, 45]). (0, 0) is city centre. Each test case is identified here as Shape [number of streets, street length, aspect ratio $H/W$, wind direction].

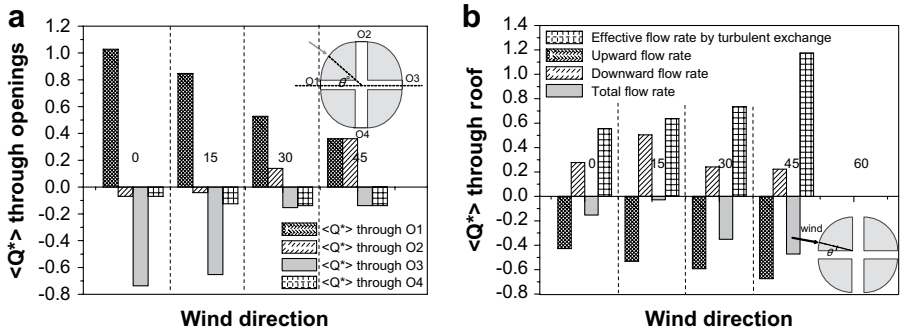


**Fig. 9.** Normalized flow rates through openings (a) and through the open roof (b) in the case Round [2, 7, 1, 0], Round [2, 7, 1, 15], Round [2, 7, 1, 30] and Round [2, 7, 1, 45]. A positive value denotes entering the street cavity and negative value denotes leaving the city. In (b), the effective flow rate by turbulent exchange on roof is only shown as the positive value. Each test case is identified here as Shape [number of streets, street length, aspect ratio $H/W$, wind direction].

dimensional streamline and the normalized velocity contour in plane of $z = 0.5H$. The borderline between the air flowing into or around the street entry O1 is separated by the two stagnation points (where velocity is zero in white color) on both windward walls. The flow pattern for a wind angle of 15° (case Round [2, 7, 1, 15]) is similar to that of for a wind angle of 0° (case Round [2, 7, 1, 0]). In both cases, the airflow enters the street through opening O1 and leaves through O2, O3 and O4. For larger wind angles of 30° and 45° (case Round [2, 7, 1, 30] and case Round [2, 7, 1, 45]), the air flows into Street 1 (Street 2) through O1 (O2), then the helical flows from Street 1 and Street 2 meet and collide each other in the Intersection, then continue into Street 3 and Street 4. The velocity in recirculation region is small.

Fig. 9 shows the normalized flow rates through openings and roofs. Fig. 9a shows an inflow rate through O1 and three outflow rates through O2, O3, O4 with 0° and 15°, however, two inflow rates through O1, O2 and two outflow rates through O3, O4 with 30° and 45°. The normalized flow rates through O1 and O3 are much larger with 0° and 15° than those with 30° and 45°. Fig. 9b shows that both upward outflow rate and downward inflow rate exist through the roof. The combined flow is outflow (i.e. upward flow) through roof in all the cases. The effective flow rate due to turbulent exchange through the street roof is always larger than that by the mean vertical flow. The vertical flow rates by both the mean flow and turbulent exchange through open roof are somewhat higher with 30° and 45° than those with 0° and 15°. Table 4 shows, for two street round cities, small angles (0° and 15°) between the approaching wind and the main street result in higher spatial mean velocity in most streets than large angles (30° and 45°).

## 4. Conclusions

The overall city form, the configuration of streets, street orientation contrast to the approaching wind direction are all shown to be significant urban morphological parameters to affect wind conditions in some simple idealized city models. Both CFD simulations and detailed wind tunnel experiments were used in this study, and there was a general agreement between the measured and predicted distribution of velocity and pressure coefficient.

We found that, the interaction between the overall city form and the approaching wind generates different flow patterns around, above and behind the city model, as a result, also has a great influence on the airflow within the street cavity. For a round city model and a square city model with two crossing streets and the parallel approaching wind, this difference results in opposite direction of the helical flow in the secondary street, i.e. the inward helical flow for the square city model and the outward helical flow for the round city model. The upward flow through the street roof is much stronger in the square city model than that in the round city model. It results in a weaker wind in street network of the square city model than that in the round city model. For a round city model with a very narrow street, the parallel approaching forward flow fails to blow through the whole street and a backward flow opposite to the approaching wind is observed through the leeward entry. The flows from two openings collide each other and leaves the street through the open roof. In a rectangular long city model, a fully developed region is approximately achieved with a steady horizontal flow along the street. This kind of flow was not observed in the short city models that we have studied. Finally, for a round city model with two crossing streets, small angles (0°, 15°) between the approaching wind and the main street may contribute to stronger wind within the entire street network.

## Acknowledgements

The work in this paper is supported by a grant from the Research Grants Council of the Hong Kong SAR Government (Project No. HKU 7145/07E). We thank Mr. R. Peltary for his help in building wind tunnel models, Mr. H. Lundstrom and Mr. L. Claesson for hotwire measurement in our wind tunnel studies. The valuable comments by Prof. James Axley, School of Architecture; School of Forestry & Environmental Studies, Yale University, USA, on the manuscript is also gratefully acknowledged.

**Table 4**
Normalized spatial average velocity $<V^*>$ in the two-street round city model of wind directions of 0°, 15°, 30°, 45°.

| Spatial mean velocity | Street 1 | Intersection | Street 3 | Street 2 | Street 4 | Entire street |
|---|---|---|---|---|---|---|
| Round [2, 7, 1, 0][a] | 0.89 | 0.78 | 0.71 | 0.27 | 0.27 | 0.56 |
| Round [2, 7, 1, 15] | 0.77 | 0.70 | 0.65 | 0.23 | 0.32 | 0.51 |
| Round [2, 7, 1, 30] | 0.53 | 0.41 | 0.22 | 0.29 | 0.24 | 0.33 |
| Round [2, 7, 1, 45] | 0.39 | 0.37 | 0.21 | 0.39 | 0.22 | 0.31 |

[a] Each test case is identified here as Shape [number of streets, street length, aspect ratio $H/W$, wind direction].

## Appendix A


**Fig. A.1.** A mosaic map of the 6th century Roman city of Jerusalem – a compact round city organized along a single wide main street. [David Bjorgen, Wikipedia Commons, 2005, under "Cardo" in Wikipedia].

## References


Belcher, S.E., Jerram, N., Hunt, J.C., 2003. Adjustment of turbulent boundary layer to a canopy of roughness elements. Journal of Fluid Mechanics 488, 369–398.

Chang, C.H., Meroney, R.N., 2003. The effect of surroundings with different separation distances on surface pressures on low-rise buildings. Journal of Wind Engineering and Industrial Aerodynamics 91 (8), 1039–1050.

Cheng, H., Castro, I.P., 2002. Near wall flow over urban-like roughness. Boundary Layer Meteorology 104, 229–259.

Cheng, Y., Lien, F.S., Yee, E., Sinclair, R., 2003. A comparison of large Eddy simulations with a standard $k$–$\varepsilon$ Reynolds-averaged Navier–Stokes model for the prediction of a fully developed turbulent flow over a matrix of cubes. Journal of Wind Engineering and Industrial Aerodynamics 91 (11), 1301–1328.

Choudhury, D., 1993. Introduction to the Renormalization Group Method and Turbulence Modeling. Fluent Inc. Technical Memorandum TM-107.

Conceal, O., Belcher, S.E., 2005. Mean winds through an inhomogeneous urban canopy. Boundary Layer Meteorology 115, 47–68.

Cowan, I.R., Castro, I.P., Robins, A.G., 1997. Numerical considerations for simulations of flow and dispersion around buildings. Journal of Wind Engineering and Industrial Aerodynamics 67, 535–545.

Fenger, J., 1999. Urban air quality. Atmospheric Environment 33, 4877–4900.

Grimmond, C.S.B., Oke, T., 1999. Aerodynamic properties of urban area derived from analysis of surface form. Journal of Applied Meteorology 38, 1262–1292.

Hamlyn, D., Britter, R.E., 2005. A numerical study of the flow field and exchange processes within a canopy of urban-type roughness. Atmospheric Environment 39 (18), 3243–3254.

Hanna, S.R., Tehranian, S., Carissimo, B., Macdonald, R.W., Lohner, R., 2002. Comparisons of model simulations with observations of mean flow and turbulence within simple obstacle. Atmospheric Environment 36 (32), 5067–5079.

Launder, B.E., Spalding, D.B., 1974. The numerical computation of turbulent flows. Computer Methods in Applied Mechanics and Engineering 3, 269–289.

Li, X.X., Liu, C.H., Leung, D.Y.C., 2005. Development of a $k$–$\varepsilon$ model for the determination of air exchange rates for street canyons. Atmospheric Environment 39, 7285–7296.

Li, Y., Stathopoulos, T., 1997. Numerical evaluation of wind-induced dispersion of pollutants around a building. Journal of Wind Engineering and Industrial Aerodynamics 67, 757–766.

Macdonald, R.W., 2000. Modelling the mean velocity profile in the urban canopy layer. Boundary Layer Meteorology 97, 25–45.

Oke, T.R., 1988. Street design and urban canopy layer climate. Energy and Buildings 11, 103.

Skote, M., Sandberg, M., Westerberg, U., 2005. Numerical and experimental studies of wind environment in an urban morphology. Atmospheric Environment 39, 6147–6158.

Soulhac, L., 2000. Modélisation de la dispersion atmosphérique à l'intérieur de la canopée urbaine. Ph.D. thesis, Ecole Centrale de Lyon.

Vitruvius, M.P., 1960. The Ten Books of Architecture. Dover, New York.

Xie, X.M., Huang, Z., Wang, J., 2006. The impact of urban street layout on local atmospheric environment. Building and Environment 41 (10), 1352–1363.